ORNL/SPR-2021/2284

Fuel Performance Analysis of Chromium-Coated Cladding under Burst Conditions

Nuclear Technology Research and Development

Prepared for
U.S. Department of Energy
Advanced Fuels Campaign

R. T. Sweet[1]
S. B. Bell[1]
K. A. Kane[1]
N. A. Capps[1]
[1]*Oak Ridge National Laboratory*

September 2021
M3FT-21OR020205023

ACKNOWLEDGMENTS

This work was supported by the Advanced Fuels Campaign of the US Department of Energy Office of Nuclear Energy. The authors would like to express appreciation to Jake Hirschhorn and Ian Greenquist (Oak Ridge National Laboratory) for their support in the review of this manuscript.

SUMMARY

To reduce the oxidation of zirconium-based alloy cladding at high temperatures, accident tolerant fuel systems have been proposed. Of the concepts identified, chromium-coated cladding has been shown to slow oxidation without greatly impacting the fuel system geometry or neutronic performance. To determine how coated-cladding tubes will perform under high-temperature accident conditions, pressurized-tube burst tests have been performed using the Severe Accident Test Station at Oak Ridge National Laboratory.

To begin modeling these tubes to better understand how the coating will impact cladding behavior, these burst tests were simulated with the BISON fuel performance code. Cladding tube surface temperatures for the burst test were developed by fitting thermocouple data into axial and azimuthal profiles, while pressure data were compared until cladding failure. The temperatures at failure and the pressure evolution show relatively good agreement between the simulation and experiment results. This is the first step of a larger effort to simulate the cladding deformation process under high-temperature transient conditions and assess the cladding margin to failure more accurately.

CONTENTS

FIGURES

TABLES

ACRONYMS

LOCA	loss-of-coolant accident
MOOSE	Multiphysics, Object-Oriented Simulation Environment
SATS	Severe Accident Test Station
Zr-4	Zircaloy-4

FUEL PERFORMANCE ANALYSIS OF CHROMIUM-COATED CLADDING UNDER BURST CONDITIONS

1. INTRODUCTION

Due to the events at the Fukushima Daiichi Nuclear Power Plant in 2011, there has been a large international effort to develop accident tolerant fuel concepts to help minimize and possibly mitigate the consequences of phenomena such as the high-temperature oxidation of zirconium-based cladding and structural materials. The zirconium oxidation reaction with the coolant is exothermic and releases hydrogen gas. As zirconium heats past 1200˚C, the oxidation reaction kinetics reach a point where the heat released from the reaction can drive a further increase in temperature, reaching a thermal feedback cycle and becoming autocatalytic. At this point, the reaction continues releasing energy and hydrogen until the metal is consumed [1, 2]. This increases the energy that needs to be removed by emergency cooling systems; as the hydrogen gas concentration increases, it may eventually ignite [3]. Multiple strategies have been proposed to improve cladding safety during a similar scenario, such as using alternative materials for fuel cladding or simply coating the outside of the current zirconium-based alloys [4]. Further, these strategies may provide enhanced safety benefits to current fuel systems, allowing them to operate more efficiently and improving the economic viability of nuclear power.

Of the current coating candidates, chromium has been selected because of its superior oxidation kinetics and its compatibility with the zirconium-based substrate [5]. Chromium forms an extremely protective oxide layer, Cr_2O_3, allowing the coating layer to be beneficial in relatively thin layers. This helps reduce the neutronic penalty from the thermal neutron absorption of chromium and allows current fuel designs to implement coated cladding without geometric reconfiguration. However, some outstanding issues need to be determined before full deployment, such as cladding-coating chemical interactions, irradiation performance, and coating performance during transient scenarios [6].

Applied coatings are expected to help improve the cladding oxidation behavior as long as they remain adherent and form a passivating oxide layer. Under a transient scenario, such as a loss of coolant accident (LOCA), the cladding may rupture because of the internal gas pressure as the fuel rod temperatures increase. During the lead up to rupture, the cladding will begin to deform, forming a ballooned region where the cladding will subsequently rupture, and the pressure will be released [3]. During this deformation process, it is expected that the coating will delaminate from the substrate or form cracks allowing water and stream ingress to the cladding surface [5]. However, the coating may provide increased structural stability to the cladding at high temperatures, thereby reducing the cladding deformation and balloon size and further prolonging cladding rupture. If true, then coatings may offer support toward the industries' high-burnup safety case and potentially result in a modification of high-burnup fuel fragmentation relocation and dispersal consequences.

To determine how these coating materials will impact the cladding performance during transient scenarios, cladding burst test experiments are simulated using finite-element modeling techniques, and the results are compared. This work leverages efforts to further characterize cladding burst behavior to support high-burnup fuels. The goals of this work are to verify that the coating has no adverse effects on the cladding during transient scenarios, identify changes of the margin to burst by comparing coated and uncoated cladding burst tests under similar conditions, and better define the temperature and strain conditions of the cladding during rupture tests to assess the cladding margin to failure more accurately.

2. MODELING APPROACH

2.1 SEVERE ACCIDENT TEST STATION DATA

Data generated from experiments performed in the Severe Accident Test Station (SATS) at ORNL are used to model the cladding conditions during the transient scenario [7]. This particular set of experiments uses a pressurized cladding tube specimen heated using an infrared furnace until the cladding ruptures. These tube samples can range in length from 6 to 12 in. and have an alumina rod (8 mm outer diameter) spanning the center of the tube. For all of the data discussed in this manuscript, 12-in. cladding segments are used. Figure 1 shows a diagram of the LOCA furnace setup on the SATS [8]. This test uses a pressure transducer to measure the in situ argon gas pressure, which is set and sealed before the cladding is heated. This is performed using an external gas tank with lines leading to a pressure regulator, shutoff valve, and pressure transducer. From here, gas lines connect to the cladding tube through a locking fitting.

The cladding is instrumented with four thermocouples, three along the "rear" axial length, and one placed 180˚ azimuthally across the midplane of the tube. The cladding tubes are heated to a holding temperature of 573 K and held for ~5 minutes, then the temperature is ramped at approximately 5˚C/s, according to a control thermocouple (in this case, the middle rear thermocouple). As the gas expands during the initial heating phase, the cladding tube balloons and bursts. This is identified through the pressure transducer data, which record a rapid depressurization. For these experiments, flowing steam heated to 673 K is injected into the chamber. The cladding is heated to ~1200˚C (1473 K) and held constant for 5 min, and then the furnace is deactivated and the cladding cools. When the cladding control thermocouple reaches 873 K, the flowing steam is shut off and the tube is quenched in room-temperature distilled water.

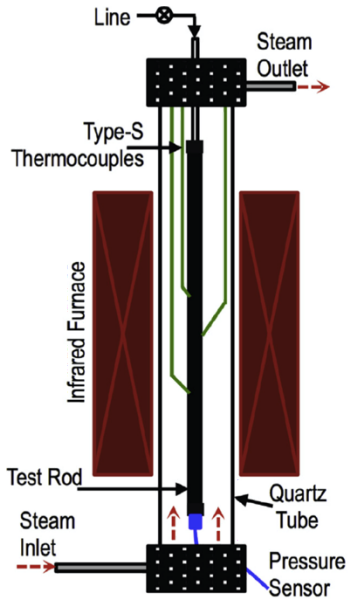

Figure 1. Diagram of the Severe Accident Test Station setup.
(*Reproduced from: C. P. Massey, et al., Journal of Nuclear Materials 470 (2016): 128-138*)

The thermocouples used across the cladding tube are placed in the central 4 in. (~10.2 cm) of the tube length. For all of the experimental tests considered here, the middle thermocouple is approximately 6 in. (~15.2 cm) up the cladding tube, and the top and bottom are 2 in. (~5.1 cm) above and below, respectively. Figure 2 shows a schematic of the thermocouple locations and the most common burst

location, the back side of the tube between the center and bottom thermocouple locations. This is important because the cladding is expected to experience the greatest deformation in the hottest region.

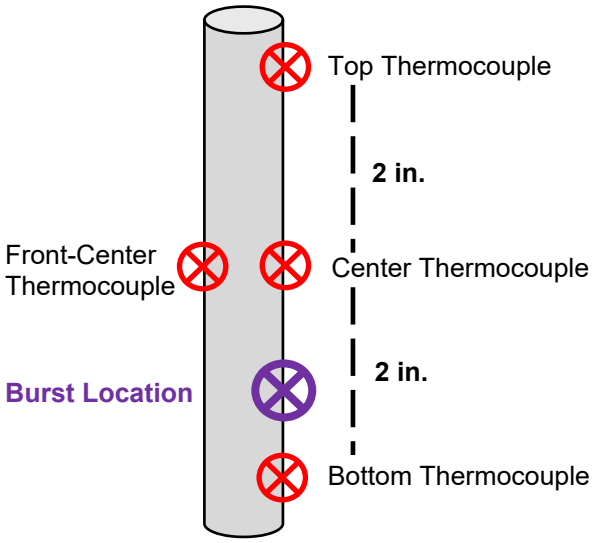

Figure 2. Schematic of the thermocouple placement and burst location on the center 4 in. (~10.2 cm) section of the 12-in. (~30.5 cm) cladding test specimen used in the Severe Accident Test Station.

These tests are run on a variety of coated and uncoated cladding tubes with various alloy substrates and with different initial pressures. The data is acquired over time from a typical cladding burst test and shown in Figure 3. The left axis of this figure shows the recorded temperatures for the four thermocouples over the first 700 s of the burst test for an uncoated Zircaloy-4 (Zr-4) tube with an initial pressure of 800 psi (~5.5 MPa). The right axis shows the data recorded by the pressure transducer. Initially, as the cladding is heated leading into the first holding stage, the pressure increases with the gas temperature. This pressure increase does not necessarily correspond to the cladding temperatures because of additional argon fill gas in the system located in fixtures and gas lines connecting to the cladding tube outside the furnace. After the holding period, the cladding temperature is ramped to simulate the LOCA transient. In this example, the rupture can be seen to occur at ~443 s by the rapid decrease in pressure and the large shift in cladding temperatures. This temperature shift is driven by the release of gas stored in the system which is cooler than the cladding. Because this work is concerned only with the bursting behavior of the cladding tube, the high temperature data and the cool down are not especially relevant and are therefore not included in this manuscript.

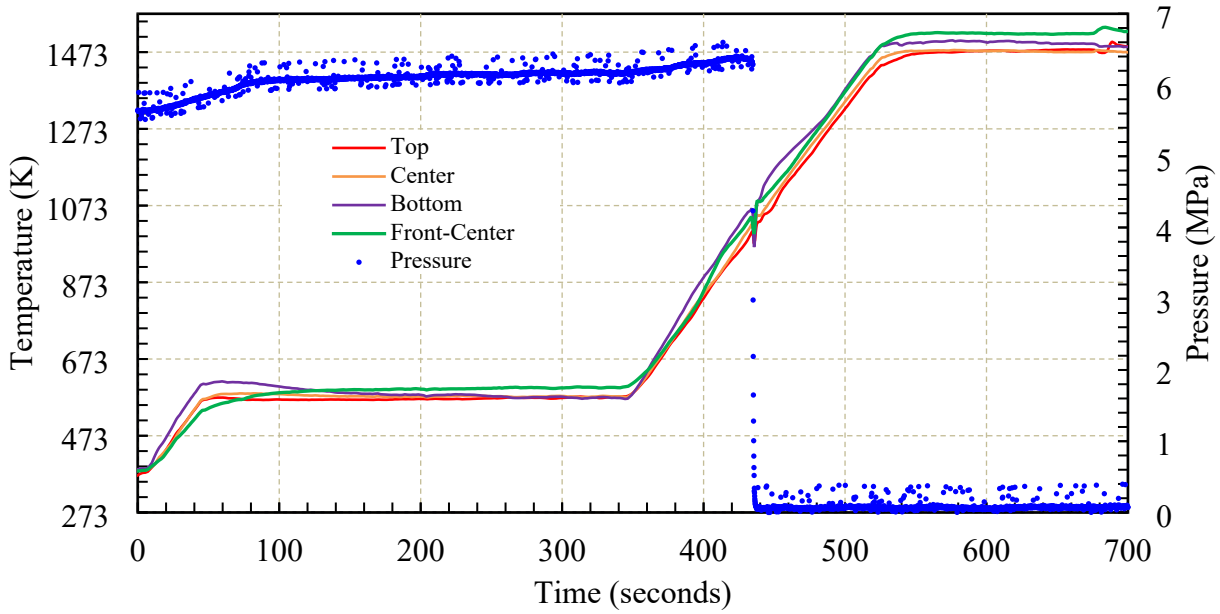

Figure 3. Example of thermocouple and pressure data generated from the uncoated, 800 psi, Zr-4 burst test.

For this analysis, two different chromium-coated/uncoated cladding tube experiment series are considered, based on their substrate composition. Table 1 shows the geometric details of the different experiments. The first series uses a 575 µm thick Zr-4 substrate; samples that are coated have a 7 µm chromium coating. In this series, sample initial pressures range from 600 to 1600 psi (4.1 to 11 MPa). The second series uses a 610 µm thick ZIRLO™ substrate where coated samples have a 6 µm chromium coating; initial pressures ranged from 150 to 1200 psi (1 to 8.3 MPa). All tests discussed here were performed using the parameters described previously.

Table 1. Summary of cladding properties and geometries used in the Severe Accident Test Station for this analysis

Cladding properties	Series #1	Series #2
Substrate material	Zr-4	ZIRLO™
Inner radius (mm)	4.175	4.135
Outer radius (mm)	4.750	4.745
Cladding thickness (mm)	0.575	0.610
Cladding length (cm)	30.48	
Coating thickness (µm) *(if applied)*	7	6

2.2 SURFACE TEMPERATURE PROFILE DEVELOPMENT

To enhance the quality of the burst testing model, the thermocouple data from the SATS experiments were modified to include a continuous shape and azimuthal variation to generate a full 3D cladding surface temperature. Traditionally, the temperature between the thermocouple locations is simply interpolated linearly, but because the cladding burst is not occurring at the thermocouple locations, presumably the actual peak temperature is not currently measured. The burst locations in these tests show a degree of reproducibility, indicating that that failure is not due to preexisting flaws/preparation.

Additionally, because the complete surface temperature is necessary to accurately calculate the cladding pressure evolution due to gas expansion, this method serves to improve the pressure calculation.

To generate the axial variation, a fourth-order polynomial is used with the thermocouple temperatures imposed as constraints. This polynomial is also fit to the cladding tube end temperatures, which have been rudimentarily measured to fall at nearly 60–80% of the nearest thermocouple temperature. This estimation comes from previous tests in the SATS using a fiber optic temperature sensor. Although this is a significant approximation, the ends of the cladding tube are much cooler than the middle sections are because of the tube placement within the furnace, and therefore the cladding tube ends will not experience significant thermal creep deformation. Figure 4 shows a selected axial temperature profile for an uncoated, 1200 psi, ZIRLO™ burst test. This case was chosen to demonstrate the temperature surface generation because it most clearly shows the increased temperature relative to the middle thermocouple. This figure shows the three thermocouple temperatures compared with the temperature profile generated using them, along with the estimated cladding end temperatures. This profile shows a peak temperature location below the lower thermocouple, which is consistent with the expectation that the peak cladding temperature should be larger in the burst location.

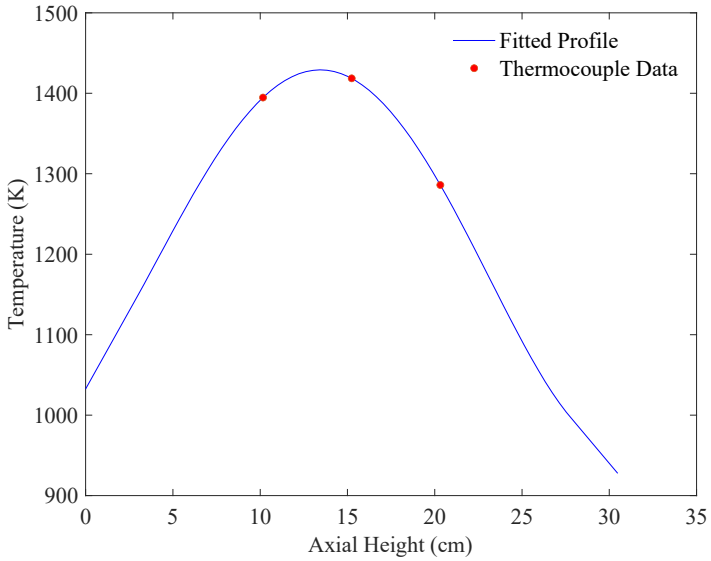

Figure 4. Example of the fitted axial profile compared with the thermocouple data generated in the Severe Accident Test Station for an uncoated, 1200 psi, ZIRLO™ burst test.

The temperature range generated from these continuous functions is shown in Figure 5. At each experiment data point acquired over time (in intervals of .1 s), the fourth-order fitting function method is used. This figure shows the range of the maximum and minimum temperatures over the experiment time. For each of these tests, the jump in the burst temperatures from the release of the stored gas at the burst time is cut out. The thermocouple temperature increase over time is interpolated linearly over these times. This is performed to ensure that the future prediction is not influenced by the temperature change from the sudden gas release from the rupture opening.

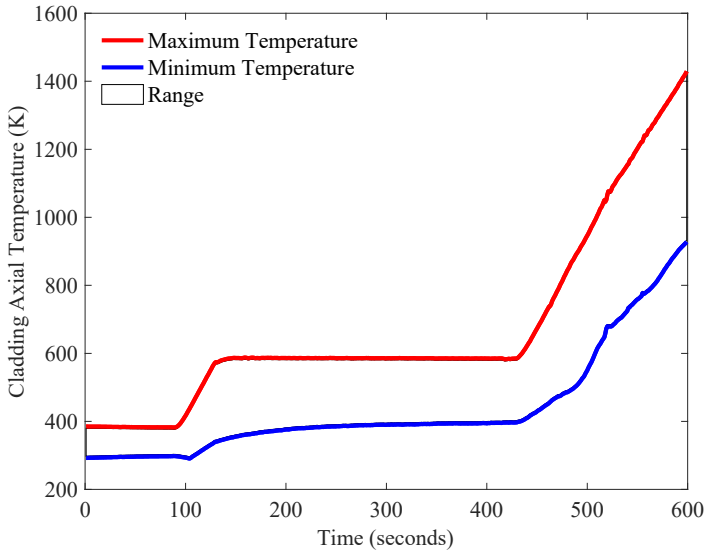

Figure 5. Example of the temperature range from the fitted axial temperature profile for the uncoated, 1200 psi, ZIRLO™ burst test.

Finally, the azimuthal thermocouple data are compared with the corresponding middle thermocouple, and a relative azimuthal thermocouple factor is calculated, indicating the relative temperature difference between the front and back of the cladding tube. In this example of the azimuthal thermocouple factor, shown in Figure 6, the rear side of the cladding is continuously hotter than the front side (as indicated by a value lower than one). The azimuthal temperature difference is incorporated into the cladding surface temperature generation through a cosine function that varies along the outer circumference of the cladding tube. This assumption produces a uniform azimuthal variation, which is not necessarily the case during these experiments; however, in the absence of thorough temperature characterization, it addresses the azimuthal temperature variation.

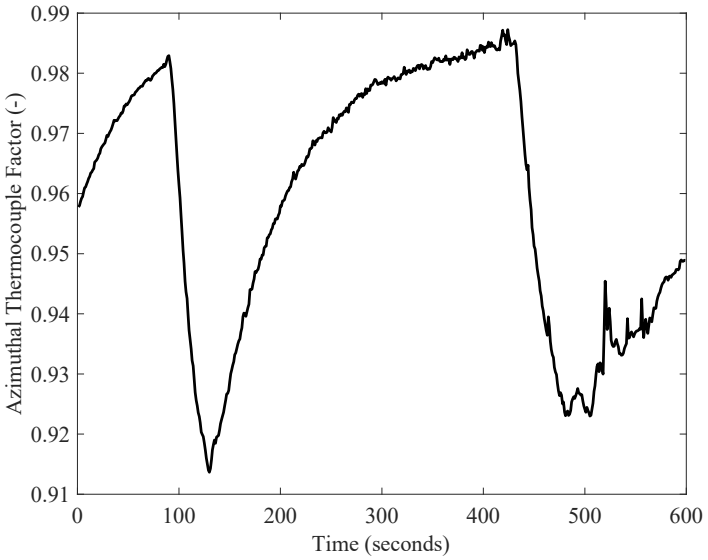

Figure 6. Example of the azimuthal thermocouple factor that reports the relative difference in the temperature from the front and back of the cladding for the uncoated, 1200 psi, ZIRLO™ burst test. A value less than 1 indicates a temperature that is hotter on the cladding back side.

Both the axial temperature profile and the azimuthal variation are used to generate a full 3D temperature surface for the cladding to be used as an input in transient simulations.

2.3 FINITE-ELEMENT MODEL

To model the cladding tube under the transient conditions, the BISON fuel performance code is used. BISON is a nuclear fuel specific, finite-element analysis code built on the MOOSE (Multiphysics, Object-Oriented Simulation Environment) Framework [9]. MOOSE employs a Jacobian-Free Newton-Krylov method to solve coupled systems of nonlinear partial differential equations with parallel computing [10]. The expandability of the MOOSE framework allows BISON to incorporate a host of materials as well as behavioral models for integral fuel performance modeling. This model consists of material-specific constitutive properties, the cladding tube geometry, and the input conditions generated from the experimental data [11].

For these simulations, previously developed constitutive properties for the alumina rod, zirconium-based claddings, and chromium coating are used. To model the alumina rod, only elastic and thermal properties (thermal conductivity, specific heat, and thermal expansion) are used [12] because the rod is assumed to have no impact on the structure of the cladding tube but may serve as a thermal sink during the heating phase. Both the cladding (Zr-4 and ZIRLO™) and chromium coating have elastic, thermal, and creep properties.

The elastic modulus, Poisson's ratio, thermal expansion strain, thermal conductivity, and specific heat are all calculated for the zirconium-based alloys using correlations from MATPRO [13]. The thermal creep model is divided into a composition-specific, low temperature correlation (after [14, 15]) and a high-temperature creep phase-dependent model (after [16]). The parameters used in the high-temperature creep model based on the material phase and the determination of the phase model are implemented from a previous work on the behavior of cladding during high-temperature transients [17]. Properties for the chromium coating include fitted data for temperature-dependent thermal conductivity, specific heat, and elastic modulus [18]. The thermal creep model used to simulate chromium is a Norton creep model fitted to data from previous thermal creep tests [18, 19]. The aforementioned models for the zirconium-based claddings and the chromium coating were developed during previous studies and are distributed with BISON.

The impact of the creep models is significant because it is the dominant deformation mechanism responsible for the cladding balloon to form. The cladding is assumed to fail when the creep rate reaches ~2.78%/s, based on previous work modeling plastic instability in fuel performance codes [20]. At this point the cladding is assumed to undergo plastic instability and begins to rapidly deform to failure. This provides an accurate comparison of the rupture temperature and time to burst; however, the cladding strain profile is greatly underpredicted [21]. For this analysis, only the engineering stress (calculated using the internal pressure) and the cladding temperatures are compared. Planned upgrades to this experimental equipment are expected to allow in situ true strain comparison between the cladding tube and simulation results.

The cladding tube geometries are generated using the parameters in Table 1. In these simulations, the coating is modeled as a distinct domain applied to the outside of the cladding with a sharp transition. As such, this model does not include any transition layers associated with the coating application, nor does this model allow delamination of the coating. These are 3D, 180˚ cladding tubes with the zero-displacement constraints on the bottom of the cladding tube and an axial slice of the cladding to prevent

rigid body motion. The half-rod symmetry used in these simulations fully incorporates the azimuthal and axial temperature variations while reducing the total computing resource usage.

In this representation, the cladding end tubes are sealed to calculate the gas volume inside the tube more easily. The internal gas volume consists of two separate volumes: (1) a volume calculated inside the tube itself, which heats and expands, increasing the internal pressure; and (2) a miscellaneous volume held at room temperature and used to represent all the extra gas in the system, such as the gas lines and fittings, valves, and pressure transducer. This miscellaneous volume is calibrated for both series of tests independently based on the measured increase in pressure during the temperature ramp. Effectively, this model is utilized as a gas reservoir that dampens the pressure changes within the cladding tube; the volume and temperature of the reservoir do not change, but the pressure remains in equilibrium with the cladding tube.

The only external conditions applied to this model are the temperature and the initial pressure. Section 2.2 thoroughly describes the process by which the cladding surface temperatures are generated for each experimental run. These temperatures are applied to the cladding surface as Dirichlet boundary conditions at each timestep. Because the simulations assess the volume, temperature, and pressure of the internal gas together from room temperature, the internal pressure is set to closely match the pressure of the burst experiments during the first holding period after the pressure regulator is set, the gas valves are closed, and the tube is sealed. These simulations operate through the first holding period until the heating phase and are terminated when the cladding creep strain rate threshold is reached.

3. RESULTS

3.1 COMPARISON WITH SATS DATA

Boundary conditions for the 3D cladding model were generated from individual cladding burst tests of coated and uncoated zirconium-based alloys and implemented into the BISON fuel performance code. An illustration of the generated temperature surface resulting from a simulation is shown in Figure 7. This shows the temperature surface at the burst temperature for the uncoated, 800 psi, Zr-4 burst test. This example shows a hotspot generated in the cladding along the front, near the lower span of the cladding tube. This local increase in the cladding tube temperature leads to a localized increase in the creep strain rate and subsequent cladding failure.

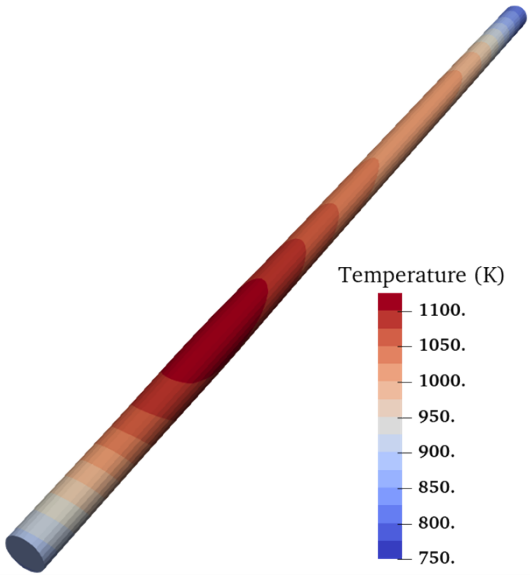

Figure 7. 3D cladding surface temperature at the rupture temperature for the uncoated, 800 psi, Zr-4 burst test; geometry is reflected into a 360° model across the axial plane to better illustrate the temperature variation.

The pressure evolution of the cladding tube during this same simulation is shown in Figure 8. In this simulation the initial pressure is 5.75 MPa (shown in blue), while the data begins at nearly 5.7 MPa (shown in red). Because of the different starting pressures, the pressure through the holding phase is slightly different; however, the pressure in the experiment slowly increases to reach a similar value before the heating phase. This is assumed to occur because of heating of the connected equipment, which may be heating the gas volume external to the cladding tube. As the heat up phase begins, the pressure in both the simulation and the experiment increases similarly. Because the simulation is terminated before extensive deformation can occur, the pressure data does not show the same shoulder that the experiment shows before the cladding ruptures. This is an effect from both the high temperature cladding creep model and the failure criteria. Though the evolution of the cladding deformation is expected to be somewhat different, the time to failure and the temperatures are quite similar, indicating good agreement in the boundary conditions used to generate this model.

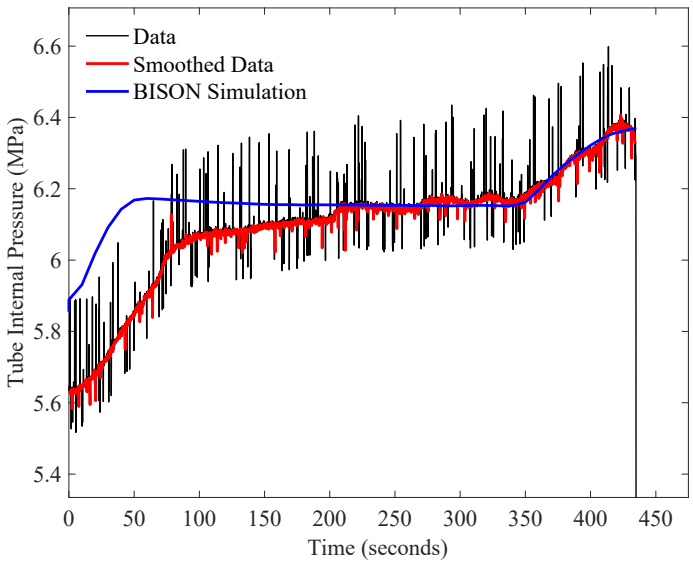

Figure 8. Comparison of the pressure evolution between the data (black), a smoothed data representation (red), and simulation (blue) for the uncoated, 800 psi, Zr-4 burst test.

This process was performed for seven ZIRLO™ cladding tubes (three coated, four uncoated) and eight Zircaloy-4 tubes (four coated, four uncoated). To compare the experiments and the simulation results, the rupture temperature and cladding hoop stress are shown in Figure 9. Because the peak temperature is not located at the thermocouple locations, the simulations (shown in red and magenta) offer a method to assess both the peak temperature (Figure 9a) and the peak thermocouple temperature (Figure 9b) that the cladding experiences. These plots delineate the cladding burst temperature and hoop stress based on whether the cladding substrate is ZIRLO or Zircaloy-4 (square vs. circle markers), simulation or data (reds vs. blues), and uncoated or coated (red and blue vs. magenta and cyan). The burst criterion from Chapman et al. [22] is shown here for illustrative purposes and is calculated using 6˚C/s. This heating rate is calculated from the average cladding surface heating rate in the simulations, although the reported control thermocouple in SATS shows 5˚C/s.

There is no discernable impact of the cladding tube material, at least between the ZIRLO and Zirclaoy-4 used in these cladding tests; this is likely due to the similarity in the creep models used, especially at high temperatures, where the models only show a difference up to 900 K due to interpolation from the creep model used for normal operation. The simulated burst tests generally predict cladding rupture temperatures much greater than the experimental temperatures, especially for Figure 9a**.** Although some points are relatively unchanged, by using the peak temperature of the cladding at rupture, the burst temperatures can be increased as much as ~20 K. This highlights a need for new temperature characterization methods to be employed during these experiments to ensure the temperature at the burst location can be determined more accurately.

Although the chromium-coated cladding burst tests are expected to show some amount of added cladding structure, the impact of the coating in these simulations is hardly discernable. These results indicate that the coating at least does not have a negative impact on the behavior of the cladding tube. This model does not include degradation mechanisms of the coating, such as cracking, delamination, or spalling, which may further diminish the impact of the coating. Given the favorable comparison of the simulations and experiment, a short parametric evaluation was performed to identify the impact of the coating on the cladding at various initial pressures.

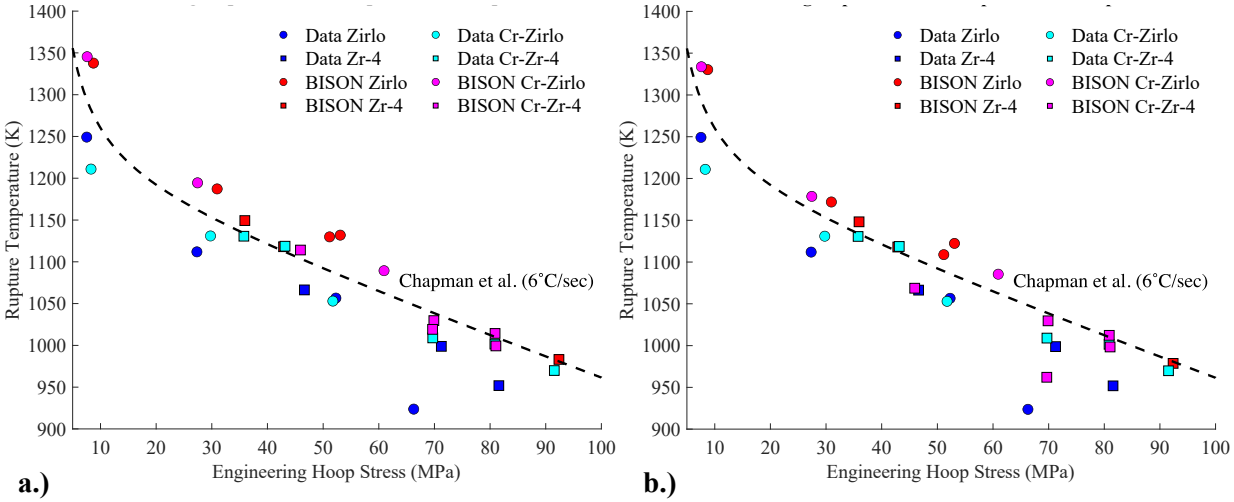

Figure 9. Cladding rupture temperature vs. engineering hoop stress for all burst tests and corresponding simulations. BISON data (red and magenta) on the left (a) use the peak temperature on the cladding surface, whereas BISON data on the right (b) use the peak thermocouple temperature to make a consistent comparison with the experimental data.

3.2 PARAMETRIC EVALUATION OF CLADDING BURST IMPACT FROM CHROMIUM COATING

To more clearly determine the impact of the chromium coating on the predicted cladding burst behavior during a transient scenario, a short parametric evaluation was performed. This set of simulations considers an uncoated and a 6 µm chromium-coated ZIRLO™ cladding tube under the same operating conditions, where only the initial pressure is varied. The temperature boundary conditions for these simulations are from the 500 psi, uncoated ZIRLO™ burst experiment. Figure 10 shows the results of this analysis where the initial pressure was varied from 3 to 15 MPa in 1 MPa increments. In this figure, the rupture temperature is the peak cladding temperature, and the lower error bars represent the peak thermocouple temperature. The results of this analysis demonstrate that the 6 µm thick chromium coating can provide an approximately ~10 K increase in the burst temperature. While that is not significant, it shows that at the very least there are no adverse thermomechanical effects using the current simulation models, and it highlights the potential for an increased burst temperature margin from thicker coatings. Additional work will need to be performed to determine the impact of intermediate phases that may form between the coating and the cladding. These results also show an increase of ~5–25 K by using the peak temperature instead of the peak thermocouple temperature for the burst criteria. This again highlights the need for consistency among the temperatures used to delineate rupture and the need for additional temperature characterization in these experiments.

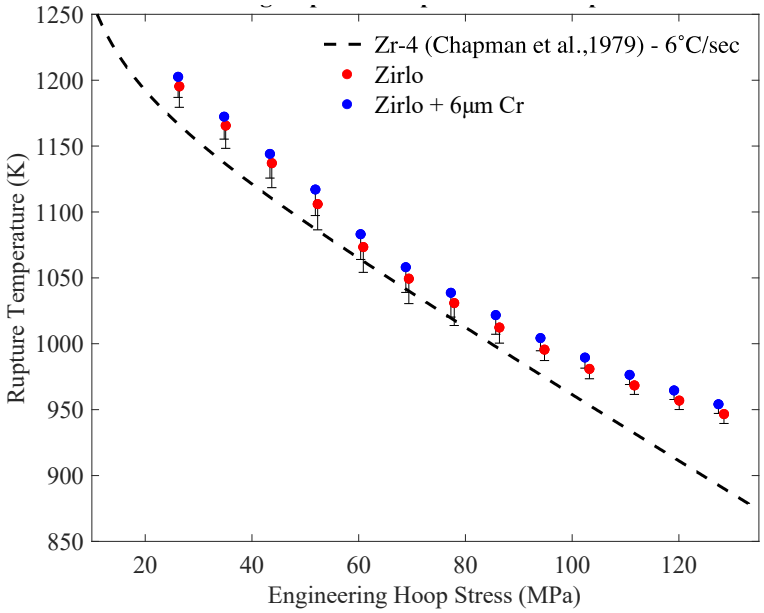

Figure 10. Coated (blue) cladding simulations show an increased rupture temperature relative to uncoated (red) cladding. Marker temperatures show the maximum cladding temperature, and error bars show the peak thermocouple temperature.

4. CONCLUSIONS AND FUTURE WORK

To assess the conditions where cladding burst may occur more accurately, additional characterization of the cladding temperatures in these experiments is necessary. Improvements to the LOCA furnace are planned, which should allow the *in-situ* measurement of the cladding strain, through a digital image correlation system, as well as full surface temperature acquisition from a thermal imaging system.

This work demonstrated a method to develop a full cladding tube surface temperature distribution, which was used as a boundary condition to make comparisons to cladding burst experiments. Whereas the temperatures at failure and the pressure evolution show relatively good agreement, this is the first step of a larger effort to simulate the cladding deformation process and assess the cladding margin to failure more accurately. This is important to assess the performance of coated cladding materials and is also beneficial for high-burnup fuels, which are expected to have higher rod internal pressures.

Future work for this assessment of coating performance includes a comparison of the cladding strain profiles between the simulation and experiment and the eventual implementation of a new cladding creep model, which is expected to simulate the cladding behavior at high temperatures more accurately. Additionally, identifying any impacts of the coating that arise during steady-state operation is also planned. This includes the implementation of irradiation properties of the coating and a power-law strain hardening plasticity model. These models will then be applied to a full-length rod analysis to compare steady-state performance impacts from coated cladding.

5. REFERENCES

1. Cathcart, J., et al., *Zirconium metal-water oxidation kinetics. IV. Reaction rate studies*. 1977, Oak Ridge National Lab.
2. Moalem, M. and D.R. Olander, *Oxidation of Zircaloy by steam.* Journal of Nuclear Materials, 1991. **182**: p. 170-194.
3. Hofmann, P., *Current knowledge of core degradation phenomena, a review.* Journal of Nuclear Materials, 1998. **270**: p. 194-211.
4. Terrani, K., *Accident tolerant fuel cladding development: Promise, status, and challenges.* Journal of Nuclear Materials, 2018.
5. Brachet, J.-C., et al., *Early studies on Cr-Coated Zircaloy-4 as enhanced accident tolerant nuclear fuel claddings for light water reactors.* Journal of Nuclear Materials, 2019. **517**: p. 268-285.
6. Geelhood, K. and W. Luscher, *Degradation and Failure Phenomena of Accident Tolerant Fuel Concepts: Chromium Coated Zirconium Alloy Cladding*. 2019, Pacific Northwest National Laboratory: Richland, Washington.
7. Snead, M.A., et al., *Severe Accident Test Station Design Document*. 2015, ; Oak Ridge National Lab. (ORNL), Oak Ridge, TN (United States). p. Medium: ED; Size: 62 p.
8. Massey, C.P., et al., *Cladding burst behavior of Fe-based alloys under LOCA.* Journal of Nuclear Materials, 2016. **470**: p. 128-138.
9. Williamson, R.L., et al., *Multidimensional multiphysics simulation of nuclear fuel behavior.* Journal of Nuclear Materials, 2012. **423**(1-3): p. 149-163.
10. Gaston, D., et al., *MOOSE: A parallel computational framework for coupled systems of nonlinear equations.* Nuclear Engineering and Design, 2009. **239**(10): p. 1768-1778.
11. Hales, J., et al., *BISON Theory Manual The Equations Behind Nuclear Fuel Analysis*. 2016, Idaho National Laboratory (INL), Idaho Falls, ID (United States).
12. Auerkari, P., *Mechanical and physical properties of engineering alumina ceramics*. Vol. 23. 1996: Technical Research Centre of Finland Espoo.
13. Hagrman, D.T., C.M. Allison, and G.A. Berna, *SCDAP/RELAP5/MOD 3.1 code manual: MATPRO, A library of materials properties for Light-Water-Reactor accident analysis. Volume 4*. 1995.
14. Limbäck, M. and T. Andersson. *A model for analysis of the effect of final annealing on the in-and out-of-reactor creep behavior of zircaloy cladding*. in *Zirconium in the Nuclear Industry: Eleventh International Symposium*. 1996. ASTM International.
15. Matsuo, Y., *Thermal Creep of Zircaloy-4 Cladding under Internal Pressure.* Journal of Nuclear Science and Technology, 1987. **24**(2): p. 111-119.
16. Erbacher, F., et al., *Burst Criterion of Zircaloy Fuel Claddings in a Loss-of-Coolant Accident*, in *Burst Criterion of Zircaloy Fuel Claddings in a Loss-of-Coolant Accident*. 1982.
17. Pastore, G., et al. *Modeling of fuel behavior during loss-of-coolant accidents using the BISON code*. in *2015 LWR Fuel Performance Meeting—Top Fuel, Zurich, Switzerland*. 2015.
18. Wagih, M., et al., *Fuel performance of chromium-coated zirconium alloy and silicon carbide accident tolerant fuel claddings.* Annals of Nuclear Energy, 2018. **120**: p. 304-318.
19. Stephens, J.R. and W.D. Klopp, *High-temperature creep of polycrystalline chromium.* Journal of the Less Common Metals, 1972. **27**(1): p. 87-94.
20. Di Marcello, V., et al., *The TRANSURANUS mechanical model for large strain analysis.* Nuclear Engineering and Design, 2014. **276**: p. 19-29.
21. Capps, N.A. and R.T. Sweet, *Characterization of Modeling and Experimental Data Inconsistencies from Burst Testing for High-Burnup Commercial Fuel Rod Applications. Manuscript in Review*, 2021.

22. Chapman, R.H., et al., *Zirconium Cladding Deformation in a Steam Environment with Transient Heating*, J.H. Schemel and T.P. Papazoglou, Editors. 1979, ASTM International: West Conshohocken, PA. p. 393-408.